The Role of Nonsurface-Active Species at Interfacial Molecular Recognition by Melamine-Type Monolayers

D. Vollhardt,*,† F. Liu,†,‡ and R. Rudert§

Max Planck Institute of Colloids and Interfaces, D-14424 Potsdam/Golm, Germany, Department of Chemistry, Nanjing University, Nanjing 210093, P. R. China, and Federal Institute for Materials Research and Testing, Unter den Eichen 87, D-12200 Berlin, Germany

Received: June 7, 2005; In Final Form: July 21, 2005

The main characteristics of Langmuir monolayers are radically changed by molecular recognition of hydrogen bond nonsurface-active species. The change in the thermodynamic, phase, and structural features by molecular recognition of dissolved uracil or barbituric acid by 2,4-di(*n*-undecylamino)-6-amino-1,3,5-triazine ($2C_{11}H_{23}$-melamine) monolayers is characterized by combination of surface pressure studies with Brewster angle microscopy (BAM) imaging and Grazing incidence X-ray diffraction (GIXD) measurements. Phase behavior of the $2C_{11}H_{23}$-melamine monolayer and morphology of the condensed phase domains are changed drastically, but in a specific way, by molecular recognition of uracil or barbituric acid. The main characteristics of the interfacial system can be essentially affected by the kinetics of the recognition process. Pure $2C_{11}H_{23}$-melamine monolayers show only small compact, but nontextured domains. The monolayers of $2C_{11}H_{23}$-melamine−uracil assemblies develop well-shaped circular condensed-phase domains having an inner texture with alkyl chains essentially oriented parallel to the periphery and having a striking tendency to two-dimensional (2D) Ostwald ripening. The $2C_{11}H_{23}$-melamine−barbituric acid monolayers form large homogeneous areas of condensed phase that transfer at smaller areas per molecule to a homogeneous condensed monolayer. BAM imaging of corresponding assemblies with $((CH_3(CH_2)_{11}O(CH_2)_3)_2$−melamine having modified alkyl chains demonstrates the specific effect of the monolayer component. GIXD results reveal that molecular recognition of pyrimidine derivatives gives rise only to quantitative changes in the two-dimensional lattice structure. The striking differences in the main characteristics between the supramolecular species are related to their different chemical structures. Quantum chemical calculations using the semiempirical PM3 method provide information about the different nature of the hydrogen-bonding-based supramolecular structures.

Introduction

A current goal of supramolecular chemistry is to find methods to control the assembly of molecules into larger structures.[1,2] Hydrogen bonds play an important role in the formation of highly ordered molecular architectures because of its directional preference and specific interaction.[3] Accordingly, many processes of biological molecular recognition, such as replication of nucleic acids, preservation of tertiary protein structure, and specific enzyme recognition, are essentially affected by complementary hydrogen bondings.[4−6] The specific composition of two various molecular components on the basis of the principle of the molecular recognition should result in systems with new properties and functions. According to the successful design of crystalline architectures[7] by the combination of derivatives of melamine and barbiturates,[8−10] the attention has been focused on artificial recognition models with high effectiveness of complementary hydrogen bonds in melamine-type systems.

One interesting approach is to use two-dimensional (2D) arrangements at the air−solution interface to regulate the recognition process by incorporating strong directional interactions of hydrogen bonds with a dissolved component for the manufacture of thin films.[11,12] So far, numerous interfacial recognition systems on the basis of complementary hydrogen bonding has been designed by Kunitake et al.[13] Of course, it has also been reasonable to synthesize and use amphiphilic melamine derivatives as a host component in monolayers and bilayers for interfacial molecular recognition of barbiturates.[14−17]

Despite the impressive progress in conceiving a large variety of novel supramolecular systems, there is nearly no knowledge about the in situ phase and structural properties of the amphiphilic host monolayers and in which way those are affected by molecular recognition of a guest component dissolved in the aqueous subphase. Merely Shimomura et al.[18] used microscopic fluorescence imaging to study the binding of aqueous nucleosides to a cytosine-functionalized monolayer in a special case.

The objective of the present work is to provide a contribution for filling this gap. In a recent work, we demonstrated the drastic change of all characteristics of a selected amphiphilic melamine-type monolayer by molecular recognition of a selected nonsurface-active pyrimidine derivative dissolved in the aqueous subphase on the basis of hydogen bonding; that means the recognition of nonsurface-active thymine dissolved in the aqueous subphase by 2,4-di(*n*-undecylamino)-6-amino-1,3,5-triazine ($2C_{11}H_{23}$-melamine) monolayers.[19] An optimal characterization of the differences in the structural and phase behavior

* Corresponding author. E-mail: vollh@mpikg-golm.mpg.de.
† Max Planck Institute of Colloids and Interfaces.
‡ Department of Chemistry, Nanjing University, Nanjing 210093, P. R. China.
§ Federal Institute for Materials Research and Testing, Unter den Eichen 87, D-12200 Berlin, Germany.

10.1021/jp053041w CCC: $30.25
Published on Web 08/20/2005

at the interfacial recognition process is possible by a combination of surface pressure studies with Brewster angle microscopy (BAM) imaging and grazing incidence X-ray diffraction (GIXD) measurements. In the present work, the role of the binding faces of the nonsurface-active pyrimidine derivatives is demonstrated by the comparison of uracil and barbituric acid as the nonsurface-active component in the supramolecular assemblies. Uracil has only one binding face, whereas barbituric acid has two binding faces. The experimental results are supported by a comparison of the binding energy of the host−guest entities obtained by quantum-chemical semiempirical calculations. Information about the specific contribution of the host component to the studied host−guest monolayers provides a comparison with the condensed phase textures of a similar melamine type ($(CH_3(CH_2)_{11}O(CH_2)_3)_2$−melamine), the amphiphilic alkyl chain of which is modified.

Experimental Section

The synthesis of the amphiphilic 2,4-di(*n*-alkylylamino)-6-amino-1,3,5-triazines ($2C_nH_{2n+1}$-melamine) was performed according to the scheme:

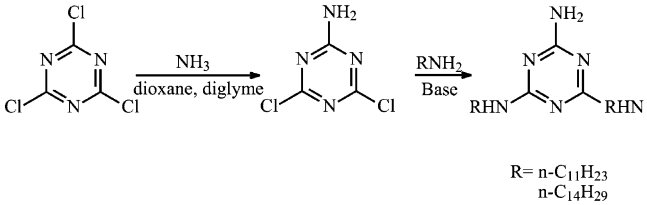

2-Amino-4,6-dichloro-1,3,5-triazine was prepared by slow bubbling of ammonia (NH_3) into a slurry of cyanuric acid chloride and diglyme in dioxane cooled in an ice−water bath (T < 10 °C) according to refs 8, 20. The obtained 2-amino-4,6-dichloro-1,3,5-triazine was used to synthesize $2C_{11}H_{23}$-melamine by aminoalkylation with undecylamine in water-free dioxane. A white final product (purity >99%) was obtained after recrystallization in ethanol and heptane.

$(CH_3(CH_2)_{11}O(CH_2)_3)_2$−melamine synthesized by Dr. Kawasaki, Japan[16,17] was a gift from him. Uracil (p.a., puriss. ≥ 99.0%) and barbituric acid (p.a., puriss. ≥99.5%) obtained from Fluka, Sigma-Aldrich Chemie GmbH were used without further purification. Ultrapure water produced by Purelab Plus was used as the subphase.

The surface pressure was measured at different temperatures using a computer-interfaced film balance with a reproducibility of ±0.1 mN/m.[21] The surface pressure−area (π−A) isotherms of the amphiphilic melamine-type monolayers spread on pure water were measured in the accessible temperature range. The monolayers were spread at an area of ∼1 nm^2/molecule, and the compression started after 10 min, sufficient for the evaporation of the spreading solvent.

Imaging of the monolayers was performed with a Brewster angle microscope (BAM 2, NFT, Göttingen), coupled to the film balance. The microscope is equipped with a special scanning technique for providing sharp images. To obtain BAM images real in scale and angle, the CCD sensor of the camera is tilted according to the Scheimpflug condition. The application of a green laser (Uniphase, San Jose, CA) allows a resolution of the BAM images of ∼3 μm.

The grazing incidence X-ray diffraction (GIXD) experiments were made on the liquid−surface diffractometer at undulator beamline BW1 in HASYLAB at DESY, Hamburg, Germany. For reducing the background scattering, the measurements were performed in a Langmuir trough placed in a sealed helium-flushed container. The monolayer can be considered as a 2D powder. The monochromatic synchrotron X-ray beam was adjusted to strike the helium/water interface at a grazing incidence angle $\alpha_i = 0.11°$. The scattered X-ray intensity was detected by a position-sensitive detector (PSD) as a function of the vertical scattering angle α_f.[22] The intensity was recorded as a function of the horizontal scattering angle 2θ by rotating the detector around the sample. The in-plane divergence of the diffracted beam was restricted to 0.09° by a Soller collimator in front of the PSD. The scattering vector Q has an in-plane component $Q_{xy} \approx (4\pi/\lambda) \sin \theta_{xy}$ and an out-of-plane component $Q_z \approx (2\pi/\lambda) \sin \alpha_f$, where λ is the X-ray wavelength.[23,24] The intensities as a function of Q_{xy} and Q_z were least-squares fitted as a Lorentzian in the *in-plane* direction and as a Gaussian in the *out-of-plane* direction. The lattice parameters a, b, and γ, the unit cell area A_{xy}, the cross-section area of alkyl chains A_0, the tilt angle t of the long molecule axis, and the tilt azimuth ψ_{xy} are obtained from the peak positions. The lattice spacing is given by $d(hk) = 2\pi/Q_{xy}^{hk}$, where (h,k) denotes the order of the reflection. t, and ψ_{xy} are calculated from the positions of the Q_{xy} and Q_z maxima,[25] according to $Q_z^{hk} = Q_{xy}^{hk} \cos \psi_{hk} \tan t$. a, b, and γ were calculated from the lattice spacing d_{hk} and from those the unit cell area $A_{xy} = ab \sin \gamma$. $A_0 = A_{xy} \cos t$ is related to A_{xy} (area per molecule parallel to the interface) and t.

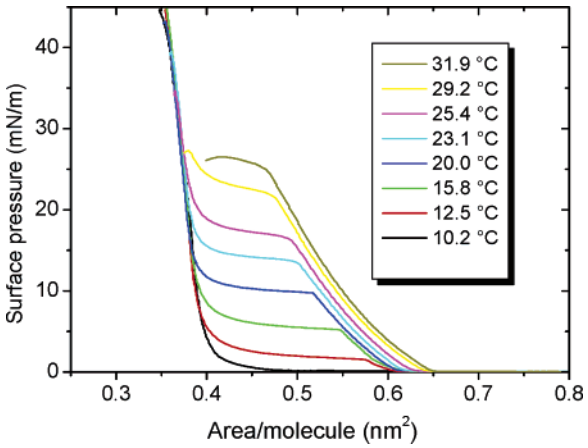

Figure 1. π−A isotherms of $2C_{11}H_{23}$-melamine monolayers spread on water measured in the temperature range between 10.2 °C and 31.9 °C.

Results and Discussion

The large effect of the nonsurface-active pyrimidine derivatives dissolved in the aqueous subphase on the thermodynamic monolayer features is already demonstrated by a comparison of the π−A isotherms. The temperature dependence of the experimental π−A isotherms of the $2C_{11}H_{23}$-melamine monolayers spread on pure water and measured with the compression rate of 0.04 nm^2/(molecule min) is illustrated in Figure 1. It is seen that the $2C_{11}H_{23}$-melamine monolayer spread on water behaves as a usual amphiphilic monolayer. The eight π−A isotherms of $2C_{11}H_{23}$-melamine monolayers recorded in the temperature range between 10.2 and 31.9 °C show a plateau (coexistence between the fluid and condensed phase) region at all temperatures. The phase-transition pressure increases and its extension decreases as the temperature increases. Thus, the precondition for the study of 2D domain morphology in Langmuir monolayers is perfectly fulfilled by the $2C_{11}H_{23}$-melamine monolayers.

Figure 2 shows the π−A isotherms of $2C_{11}H_{23}$-melamine monolayers spread on a 0.5 mM aqueous uracil subphase and

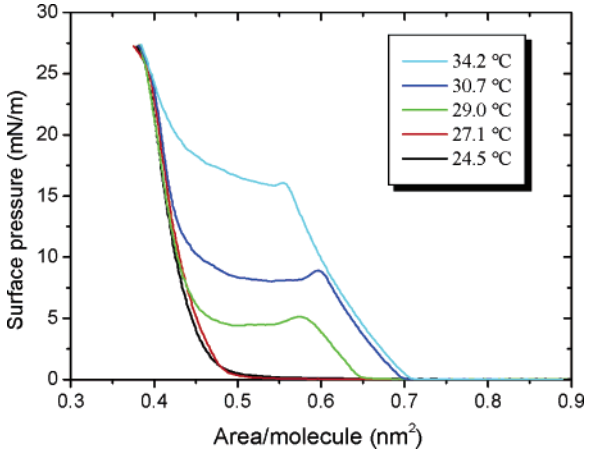

Figure 2. $\pi-A$ curves of $2C_{11}H_{23}$-melamine monolayers spread on 0.5 mM aqueous uracil subphase measured in the temperature range between 24.5 and 34.2 °C; compression rate: 0.04 nm²/(min molecule).

recorded at the same compression rate of 0.04 nm²/(molecule min) as those spread on water (see Figure 1). Clear differences between both systems indicate the effect of the nonsurface-active uracil.

At spreading on 0.5 mM aqueous uracil subphase, the plateau already disappears at 27.1 °C (Figure 2). Above this temperature, the $\pi-A$ isotherms show a plateau region, but contrary to the isotherms of the $2C_{11}H_{23}$-melamine monolayers spread on water, the extension of the plateau remains constant or even increases as the temperature increases. Small film pressure maxima at the phase-transition pressure π_c indicate supersaturation effects. Additional surface pressure studies suggest that these unusual features cannot be attributed directly to the development of a new fluid/condensed-phase coexistence of host−guest structures formed as a result of molecule recognition of the dissolved uracil. Rather, the changed features of the plateau are due to the residual material of the host monolayer that have not yet completely reacted with the dissolved uracil at the used compression rate of 0.04 nm²/(molecule min).

To obtain more information about the effect of the recognition kinetics for the dissolved component, the $\pi-A$ curves of a selected system were recorded at different compression rates, and the constant surface pressure relaxation of the area per molecule was studied. This can be supported by repeated $\pi-A$ compression/decompression curves of $2C_{11}H_{23}$-melamine monolayers spread on 0.5 mM aqueous uracil subphase and performed at the same compression/decompression rate as before. At all temperatures (e.g., $T = 29$ °C) where a plateau occurs in the $\pi-A$ curve of Figure 2, large differences exist between the compression and the decompression curve of the first cycle (Figure 3a). The plateau disappears in the decompression curve of the first cycle. At compression of the second cycle, a plateau cannot be observed, and the difference between curves at compression and decompression is largely reduced. At lower temperatures (e.g., at 25 °C in Figure 3b), where the plateau is absent in the $\pi-A$ curve of Figure 2, the hysteresis of the first cycle is small, and the curves of compression and decompression, as well as of the first and second cycles, approach to each other. The kinetic process of molecular recognition of the dissolved uracil is obviously completed when the plateau region in the $\pi-A$ curves disappeared. This can be achieved by sufficiently slow compression rates (e.g., 0.01 nm²/(molecule min). The higher their concentration, the quicker are the bonding kinetics of the dissolved component.

Molecular recognition of other pyrimidine derivatives changes the $\pi-A$ isotherms of $2C_{11}H_{23}$-melamine monolayers in a

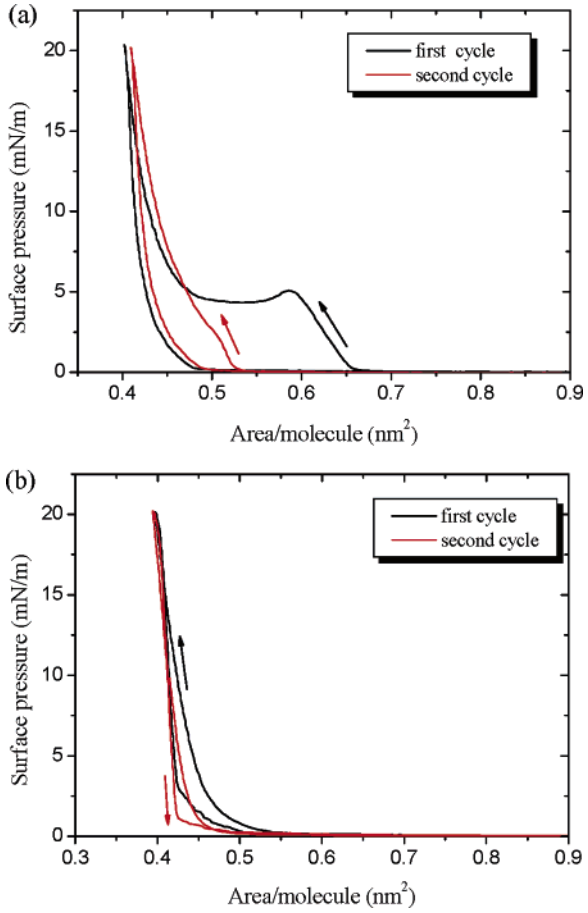

Figure 3. Two repeated $\pi-A$ compression/decompression cycles of $2C_{11}H_{23}$-melamine monolayer spread on 0.1 mM aqueous uracil subphase (a) Measured at 29 °C. Large differences exist between the compression and the decompression curve of the first cycle. That difference is small in the second cycle, the isotherms of which resemble the decompression curve of the first cycle. (d) Measured at 25 °C. At this temperature, the plateau is absent in the $\pi-A$ curve of Figure 2. Then, the hysteresis of the first cycle is small, and the curves of compression and decompression as well as of the first and second cycles approach to each other.

similar way as uracil. Recent studies of the recognition of dissolved thymine have shown that the system achieves equilibrium only at a sufficiently slow compression rate.[19] The plateau of the corresponding $\pi-A$ isotherm disappears completely under these conditions. The process of the molecular recognition of the dissolved thymine is completed obviously only in this state. This is shown by a comparison of the $\pi-A$ isotherms of the $2C_{11}H_{23}$-melamine monolayer spread on pure water, on 0.5 mM aqueous uracil subphase, and on a 0.01 mM aqueous barbituric acid subphase at a compression rate of 0.01 nm²/(molecule min) and 25 °C (Figure 4). Under these conditions, the kinetic process of molecular recognition of the dissolved pyrimidine derivatives is completed. As discussed above, the phase behavior of the $2C_{11}H_{23}$-melamine monolayer spread on pure water resembles that of a typical amphiphilic monolayer with an inclined plateau region, indicating a two-phase coexistence at $\pi \sim 16$ mN/m. The presence of the pyrimidine derivatives uracil or barbituric acid in the aqueous subphase changes drastically the shape of the $\pi-A$ isotherm and, thus, the phase behavior of the monolayer.

The presence of both pyrimidine derivatives in the aqueous subphase leads to disappearance of the plateau region and the onset of a steep pressure increase at essentially smaller area values per molecule when the molecular recognition process

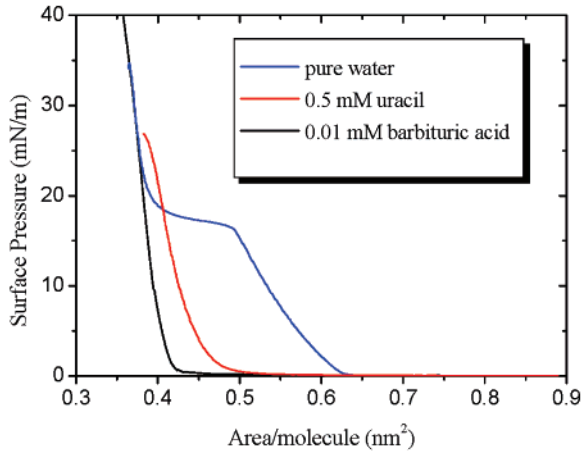

Figure 4. Comparison of the $\pi-A$ isotherms of the $2C_{11}H_{23}$-melamine monolayer spread on pure water, on 0.5 mM aqueous uracil subphase, and on a 0.01 mM aqueous barbituric acid subphase at 25 °C.

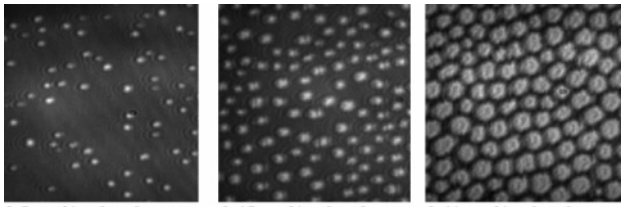

Figure 5. Domain growth in the plateau region of the $\pi-A$ isotherms measured at compression of $C_{11}H_{23}$-melamine monolayers spread on water; compression rate: 0.04 nm^2/(min molecule) $T = 20$ °C; image size: 400 μm × 400 μm.

of the dissolved pyrimidine derivatives is completed (see Figure 4). This holds for a large accessible temperature range. The strong change in the phase behavior indicates changes in the $2C_{11}H_{23}$-melamine monolayer structure by molecular recognition of the nonsurface-active pyrimidine derivatives dissolved in the subphase under formation of a supramolecular entity at the air−water interface. It is, however, interesting to note that the subphase concentration necessary to equilibrium isotherms is much lower for barbituric acid than that for uracil. It is also seen in Figure 4 that the equilibrium $\pi-A$ isotherms of the $2C_{11}H_{23}$-melamine monolayer spread on uracil and barbituric acid are not identical. Rather, the shift of the steep pressure increase to lower areas indicates a more condensed state in the case of the barbituric acid recognition.

Brewster angle microscopy (BAM) is an optimal method to visualize the high specific morphology at the molecular recognition of pyrimidine derivatives by amphiphilic melamine-type monolayers. For visualizing the effect of molecular recognition of the nonsurface-active pyrimidine derivative, the formation of the condensed phase domains of the $2C_{11}H_{23}$-melamine host monolayer, spread on water, is first considered at 20 °C (Figure 5). At the beginning of the plateau region of the $\pi-A$ isotherm, numerous small domains are formed after the phase-transition point (Figure 5, left). At further compression of the monolayer, the domains grow to an essentially larger compact size but they are nontextured (middle and right). The domain morphology is not essentially affected by temperature change and is identical to that obtained for lower compression rates, as at the compression rate of 0.04 nm^2/(molecule min), the $2C_{11}H_{23}$-melamine monolayers spread on water are in equilibrium.

The morphology of the condensed phase changes drastically when the $2C_{11}H_{23}$-melamine monolayer is spread on the aqueous subphase of a pyrimidine derivative. The large differences in

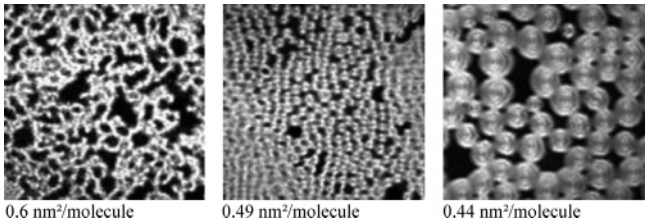

Figure 6. Development of real domain shapes at continuous compression (0.02 nm^2/(min molecule) of $2C_{11}H_{23}$-melamine monolayers spread on 0.2 mM uracil subphase; $T = 20$ °C; image size: 400 μm × 400 μm.

the specific features of the formed condensed phase textures are demonstrated for the case of molecular recognition of uracil or barbituric acid dissolved in the aqueous subphase. Figure 6 shows the domain formation of a $2C_{11}H_{23}$-melamine monolayer spread on 0.2 mM uracil subphase at the reduced compression rate of 0.02 nm^2/(molecule min) and 20 °C.

Under these conditions, the bonding kinetics of uracil approaches equilibrium and the corresponding $\pi-A$ isotherm is nearly identical to that shown in Figure 4 for 25 °C. The molecular recognition of the dissolved uracil is already completed at zero pressure. The domain formation begins at much larger areas per molecule than that for the onset of the pressure increase. The first small domains are observed at ~0.8 nm^2. At further compression, many very small domains tend to coalesce under formation of a fractal-like branched system (Figure 6, left). Then, with decreasing area per molecule, the number of newly formed small domains increases considerably and obviously prevents the domain growth (Figure 6, middle). Here, the tendency to form circular shapes can already be seen despite bridging between many individuals. Finally, at compression to some surface pressure (e.g., 7.5 mN/m in Figure 6, right) the very small condensed phase domains are transformed to essentially larger circular domains. Here, it is seen that the domains have an inner texture and the bridging tendency is partially reduced. When approaching a tight monolayer package, the distinct growth of the domains is related with a reduction of their number. According to the tendency of these systems to coalescence, this process is a matter of two-dimensional Ostwald ripening, i.e., the growth of large domains at the cost of small ones. This behavior becomes much more clearly obvious by using with a 0.5 mM uracil subphase a higher concentration of the dissolved guest component (Figure 7). Now, the recognition kinetics can already be finished at the higher compression rate of 0.04 nm^2/(min molecule) at 25 °C. Even far from the increase of surface pressure, again, a large number of small domains is formed because of the high nucleation rate governed by the high subphase concentration (see, e.g., Figure 7, 0.55 nm^2/molecule). Here, the tendency to aggregation can also be seen. These small domains are already transformed to large, approximately circular domains with pronounced inner texture at the onset of the surface pressure increase (0.3 mN/m) (see e.g., Figure 7, 0.49 and 0.48 nm^2/molecule). Finally, when approaching the tight monomolecular package, the large domains occur exclusively (see, e.g., Figure 7, 0.43 nm^2/molecule). Despite visible deformation of the domain shape due to the external pressure applied, the inner texture remains preserved.

The brightness changes within the domains represent corresponding changes in the azimuthal long-range orientation of the molecule around the center. Only sections of the domains, wherein the alkyl chains are oriented parallel to the plane of incidence, reflect the incident p-polarized light without a change of polarization.[26] The incidence plane is horizontal in the images. That means the alkyl chains are oriented essentially parallel to

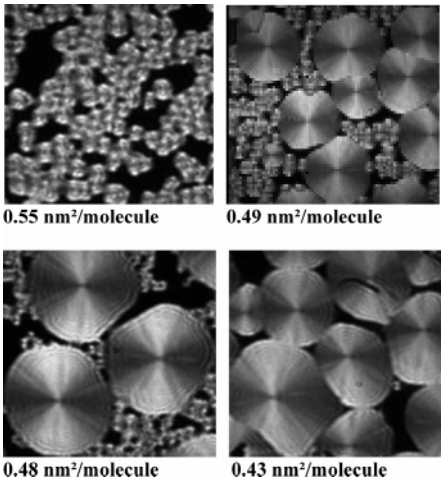

Figure 7. Two-dimensional Ostwald ripening of the domains at continuous compression (0,04 nm^2 min^{-1} $molecule^{-1}$) of $2C_{11}H_{23}$-melamine monolayers spread on 0.5 mM uracil subphase; $T = 25$ °C; image size: 400 μm × 400 μm.

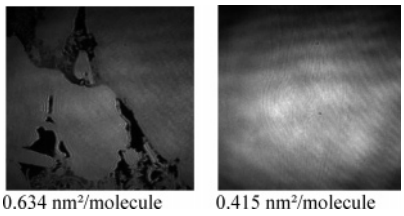

Figure 8. Formation of large homogeneous areas of condensed phase (left), finally, of a homogeneous layer of condensed phase (right) of $2C_{11}H_{23}$-melamine monolayer spread on 0.01 mM barbituric acid subphase; $T = 25$ °C; image size: 400 μm × 400 μm.

the periphery of the circular domains. Although generally the brightness and, thus, the orientation change continuously, some observable radial brightness stripes indicate also the presence of radial defect lines. Such irregularities in the long-range orientation order are facilitated if the alkyl chains are only weakly tilted. The comparatively weak optical anisotropy of the domains indicates that indeed, the alkyl chains are only weakly tilted. This conclusion is later evident by the lattice data of the interfacial $2C_{11}H_{23}$-melamine−uracil assemblies.

In the case of barbituric acid dissolved in the aqueous subphase, the concentration necessary to form host−guest assemblies with completely changed texture of the condensed monolayer phase in a measurable time interval is unusually small. The small 0.01 mM barbituric acid concentration already leads to the formation of large homogeneous areas of condensed phase at areas per molecule (0.634 nm^2/molecule) essentially larger than that for the onset of the pressure increase at the medium compression rate of 0.04 nm^2/(molecule min) (Figure 8, left). At further compression, a homogeneous monolayer of condensed phase is formed at nearly zero pressure (0.5 mN/m) before the steep pressure increase (Figure 8, right). This behavior deviating from that observed at the formation of $2C_{11}H_{23}$-melamine−uracil species is obviously caused by the two binding faces of the barbituric acid molecule that can form a linearly extended hydrogen-bonding network, preventing the formation of specific domain textures.

To obtain further information about the specific features of the melamine-type host−guest monolayers, it has been of interest to study whether and in which way a modification of the melamine type the domain morphology affects. For adequate BAM imaging, the structure of the amphiphilic alkyl chain was

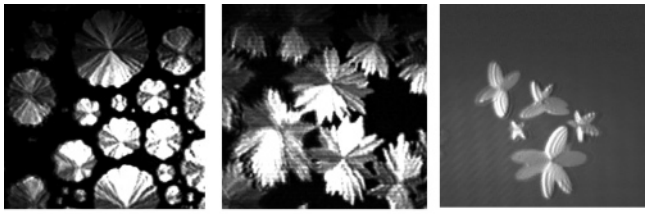

Figure 9. Molecular recognition of pyrimidine derivatives dissolved in aqueous subphase by monolayers of the modified $(CH_3(CH_2)_{11}O(CH_2)_3)_2$−melamine type; image size: 500 μm × 500 μm.

modified to $(CH_3(CH_2)_{11}O(CH_2)_3)_2$−melamine. The presence of the oxygen atom compensates the hydrophobic proportion of the additional propylene rest, so that the amphiphilic character of this compound corresponds approximately to that of $2C_{11}H_{23}$-melamine.

Figure 9 shows the domain morphology of the host−guest monolayers of the modified $(CH_3(CH_2)_{11}O(CH_2)_3)_2$−melamine type after molecular recognition of barbituric acid and uracil. Although certain similarities of the domains exist if the two differently substituted melamines form supramolecular species with the same pyrimidine derivative, there are also general differences. The concentration of the pyrimidine derivative, dissolved in the aqueous subphase and required for the formation of well-developed domain textures, is about one power of 10 higher than that necessary for $2C_{11}H_{23}$-melamine. The morphology of representative domains of the $(CH_3(CH_2)_{11}O(CH_2)_3)_2$−melamine−uracil monolayers is obviously dependent on the subphase concentration of uracil. In the case of a 3 mM uracil concentration, the domain shape is still round, but the domain boundary has numerous bulges that are coupled with defect lines directed to the center of the domain (Figure 9, left). This type of supramolecular domains resembles at most that of the circular $2C_{11}H_{23}$-melamine−uracil species, showing a similar brightness change within the domains around the center, i.e., the alkyl chains are oriented essentially parallel to the periphery of the domains. In the case of a 5 mM uracil subphase, the deviation from the circular domain shape is enlarged. Now the domain shape looks leaf-like (Figure 9, middle). The domain boundaries are sawtooth-like jagged and coupled with defect lines directed to the domain center. The azimuthal orientation of alkyl chains parallel to the domain periphery is mainly discontinuous, more or less jump-like at the defect lines. These morphology changes express an increase of the two-dimensional crystallinity as the uracil concentration in the subphase increases.

In the case of the molecular recognition of barbituric acid by the $(CH_3(CH_2)_{11}O(CH_2)_3)_2$−melamine monolayer, starlike domain shapes, admittedly with different and irregularly arranged segment numbers, are formed (Figure 9, right). The brightness distribution between the star segments indicates that the molecules are also perpendicularly oriented to the bisector of the segments. This behavior is completely different than that of the $2C_{11}H_{23}$-melamine−barbituric acid species (see Figure 8) and may be caused by a less strong hydrogen-bonding network.

Additional information about the effect of molecular recognition process on the lattice structure of the condensed phase has been obtained by GIXD studies comparing melamine-type monolayers spread on pure water and those spread on the 0.5 mM uracil subphase. Figure 10 shows the contour plots of the corrected diffraction intensities as a function of the in-plane (Q_{xy}) and out-of-plane (Q_z) components of the scattering vectors for the $2C_{11}H_{23}$-melamine monolayer spread on water (left-hand

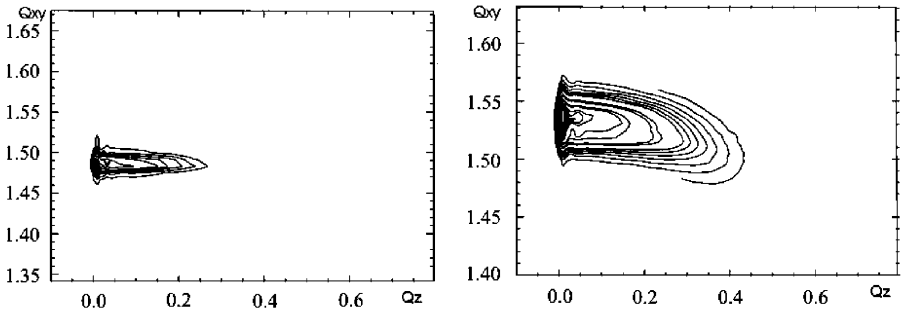

Figure 10. GIXD contour plots of the corrected diffraction intensities as a function of the in-plane (Q_{xy}) and out-of-plane (Q_z) components of the scattering vectors for a $2C_{11}H_{23}$-melamine monolayer spread on water (left) and on 0.5 mM uracil subphase (right); $T = 20°C$; $\pi = 10$ mN/m.

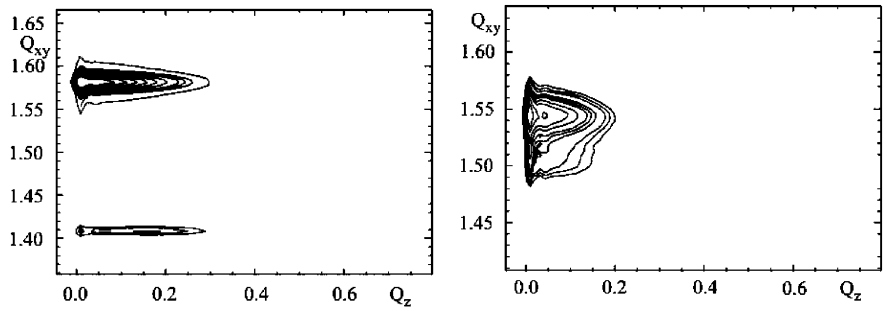

Figure 11. GIXD contour plots of the corrected diffraction intensities as a function of the in-plane (Q_{xy}) and out-of-plane (Q_z) components of the scattering vectors for a $2C_{14}H_{29}$-melamine monolayer spread on water (left) and on 0.5 mM uracil subphase (right); $T = 20°C$; $\pi = 1$ mN/m.

TABLE 1

lattice parameters for $C_{11}H_{23}$-melamine on pure water at 20 °C

surface pressure (mN/m)	a (nm)	A_0 (nm^2)	t (deg)	γ (deg)
11	0.488	0.2063	0	120
12	0.488	0.2063	0	120
20	0.487	0.2055	0	120
30	0.485	0.2039	0	120

lattice parameters for $C_{11}H_{23}$−melamine on 0.5 mM uracil at 20 °C

surface pressure (mN/m)	a (nm)	b (nm)	A_{xy} (nm^2)	A_0 (nm^2)	t (deg)	γ (deg)	tilt direction
1	0.472	0.477	0.1958	0.1950	5.4	119.6	NNN
10	0.470	0.476	0.1945	0.1937	5.3	119.6	NNN
20	0.472	0.473	0.1936	0.1930	4.5	119.9	(NNN)
25	0.472	0.471	0.1927	0.1926	2.3	119.9	(NNN)
30	0.471			0.1922	0	120	

side) and that obtained after molecular recognition of uracil dissolved in the aqueous subphase (right-hand side), both measured at 20 °C and 10 mN/m. Both contour plots seem to be similar, but in the case of the $2C_{11}H_{23}$-melamine monolayer spread on water, there is only one diffraction peak at $Q_z = 0$, whereas in the case of the $2C_{11}H_{23}$-melamine monolayer spread on a 0.5 mM uracil subphase, the diffraction peak consists of two peaks overlapping tightly to each other, both at $Q_z > 0$. The structure data calculated for these two systems are listed in Table 1, wherein a, b, and γ are the unit cell parameters, A_{xy} is the in-plane molecule area, A_0 is the cross-section area of alkyl chain, and t is the polar tilt angle. The presence of only one diffraction peak indicates hexagonal packing of perpendicularly oriented $2C_{11}H_{23}$-melamine molecules at spreading on water. Hexagonal packing exists over the surface pressure range, as seen in Table 1. The large cross-section area A_0 of the alkyl chains (only slightly decreasing with the surface pressure) indicates a rotator phase. The molecular recognition of uracil by the $2C_{11}H_{23}$-melamine monolayer also causes a change in the lattice structure, i.e., the two diffraction peaks at $Q_z > 0$ indicate a centered rectangular lattice with tilt of the alkyl chains in direction of next nearest neighbors (NNN). However, the structure data calculated for different surface pressures demonstrate that, with the increase of surface pressure, the lattice approaches that of a hexagonal structure, which is finally reached at 30 mN/m. The molecular tilt is small and the parameters a and b of the unit cell are nearly the same in the rectangular lattices.

It is interesting to note that, as found for the medium-chain amphiphilic $2C_{11}H_{23}$-melamine monolayer spread on water, a hexagonal lattice structure with a rotator phase is also formed by medium-chain dodecanol monolayers.[27] In both cases, the cross-section area of the polar headgroup is smaller than that of the alkyl chain. Therefore, the question arises in which way the lattice structure of the pure melamine-type monolayer is affected by the alkyl chain length. Therefore, comparative GIXD studies have been performed with monolayers of the homologous $2C_{14}H_{29}$-melamine spread on water and spread on aqueous 0.5 mM uracil subphase.

Figure 11 shows the corresponding contour plots of the corrected diffraction intensities as a function of the in-plane (Q_{xy}) and out-of-plane (Q_z) components of the scattering vectors measured at 1 mN/m and 20 °C, and the characteristic lattice data are listed in Table 2 for different surface pressures. The diffraction patterns of Figure 11, showing two separate peaks, are clearly different than those of Figure 10. For both systems of $2C_{14}H_{29}$-melamine spread on water (Figure 11, left) and spread on a 0.5 mM uracil subphase (Figure 11, right), the position of the two reflexes at $Q_z > 0$ (despite the small distance from zero) indicates centered-rectangular lattice with tilt of the alkyl chains in direction of next nearest neighbors (NNN). However, the similarity between them suggests that the molecular recognition of uracil gives rise only to quantitative change in the structure of the rectangular lattice in the case of this homologous $2C_{14}H_{29}$-melamine monolayer. In the case of

TABLE 2

lattice parameters for $C_{14}H_{29}$-melamine on pure water at 20 °C

surface pressure (mN/m)	*a* (nm)	*b* (nm)	A_{xy} (nm^2)	A_0 (nm^2)	*t* (deg)	γ (deg)	tilt direction
1	0.444	0.498	0.1979	0.1968	6.1	116.5	NNN
10	0.443	0.497	0.1971	0.1964	5.3	116.5	NNN
20	0.442	0.496	0.1964	0.1958	4.5	116.4	NNN
30	0.439	0.494	0.1943	0.1940	3.5	116.4	NNN

lattice parameters for $C_{14}H_{29}$-melamine on 0.5 mM uracil at 20 °C

surface pressure (mN/m)	*a* (nm)	*b* (nm)	A_{xy} (nm^2)	A_0 (nm^2)	*t* (deg)	γ (deg)	tilt direction
1	0.465	0.479	0.1947	0.1946	2.4	119.1	NNN
10	0.465	0.477	0.1938	0.1937	2.2	119.1	NNN
20	0.464	0.475	0.1925	0.1924	1.9	119.2	NNN
25	0.464	0.475	0.1925	0.1924	1.8	119.2	NNN

the pure $2C_{14}H_{29}$-melamine monolayer, the polar tilt angle *t* is small and decreases further as the surface pressure increases. However, *t* is even smaller after molecular recognition of uracil, and at high surface pressures, it approximates to zero, that is, to nearly perpendicular orientation of the alkyl chains. The lattice parameters *a* and *b* are nearly equal so that the deviation from the hexagonal structure is only small. For both homologous $2C_nH_{2n+1}$-melamine monolayers, the cross-section area A_0 of the alkyl chains diminishes as result of the molecular recognition of uracil.

The differences between interfacial assemblies formed by molecular recognition of uracil and barbituric acid can be discussed on the basis of the different chemical structures. The headgroup of 2,4-di(*n*-undecylamino)-6-amino-1,3,5-triazine ($2C_{11}H_{23}$-melamine) has two binding faces on both sides. The binding faces of uracil and barbituric acid are different. Uracil has only one binding face so that, at interfacial molecular recognition, complementary hydrogen bonding of two uracil molecules by one $2C_{11}H_{23}$-melamine molecule should be expected. On the other hand, barbituric acid has two binding faces on the same plane as $2C_{11}H_{23}$-melamine. This results in a linear extension of the hydrogen bond interaction under formation of a linear supramolecular network at the air−water interface. The chemical structure of the two different supramolecular species is shown in Figure 12.

According to the chemical structures of the assembly discussed above, the following procedure was used to calculate the hydrogen bond energy between one $2C_{11}H_{23}$-melamine molecule and two uracil molecules as well as two $2C_{11}H_{23}$-melamine molecules and two barbituric acid molecules.

In the case of the supramolecular uracil−$2C_{11}H_{23}$-melamine−uracil structure, the geometry of the three hydrogen-bonded molecules were optimized (Figure 13a), and in the case of the supramolecular $2C_{11}H_{23}$-melamine−barbituric acid structure, the geometry of each two molecules bonded in alternating sequence were optimized (Figure 13b) regarding the minimum PM3 binding energy.[28] The PM3 binding energy contains the interaction energy between all electrons and atomic nuclei in the molecule(s) with the energy of the isolated atoms subtracted. Thermal motion is neglected.

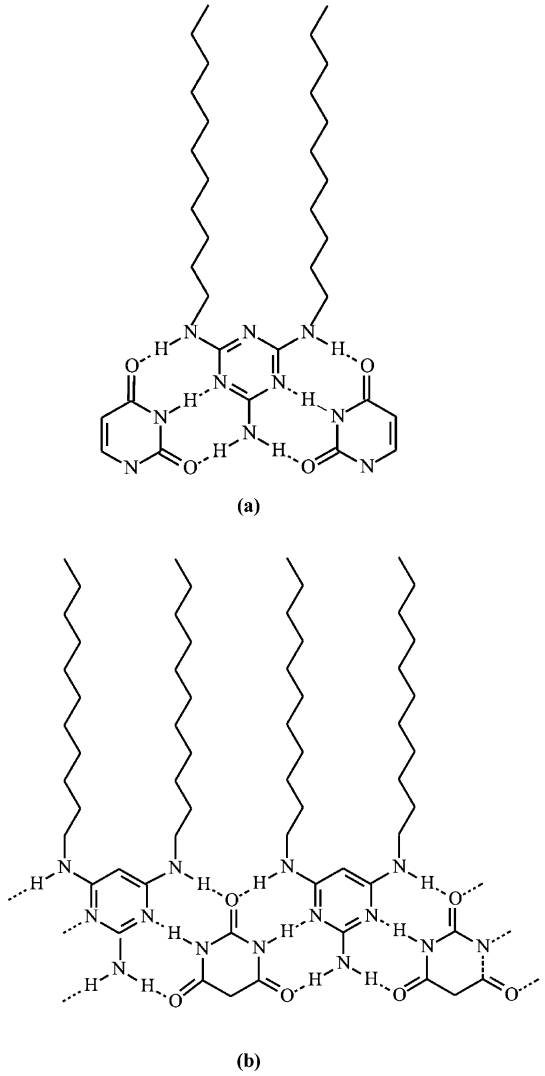

Figure 12. Chemical structure of interfacial supramolecular assemblies between 2,4-di(*n*-undecylamino)-6-amino-1,3,5-triazine ($2C_{11}H_{23}$-melamine) and pyrimidine derivatives dissolved in the aqueous subphase (a) uracil, (b) barbituric acid.

In both cases, the energy of the complexes, $E_{complex1}$ and $E_{complex2}$, respectively, was calculated. In the first case, one uracil molecule was separated from the complex, and without new optimization, the energies of the isolated uracil molecule, E_{uracil}, and that of the rest of the complex, $E_{complex1-uracil}$, were calculated. In the other case, one barbituric acid molecule was separated from the complex, and the energies of the isolated barbituric acid molecule, E_{barb}, and that of the rest of the complex, $E_{complex2-barbituric\ acid}$, were determined (Table 3). The differences E_{H1} and E_{H2} represent the hydrogen bond energy

TABLE 3

molecules	PM3 binding energy [kJ/mol]
uracil−$2C_{11}H_{23}$-melamine−uracil	−43004.88
uracil	−5459.96/−5460.22
uracil−$2C_{11}H_{23}$-melamine	−37513.07/−37512.18
barbituric acid−$2C_{11}H_{23}$-melamine−barbituric acid−$2C_{11}H_{23}$-melamine	−76088.76
barbituric acid	−5944.91/5940.32
$2C_{11}H_{23}$-melamine−barbituric acid−$2C_{11}H_{23}$-melamine	−70109.43
barbituric acid−$2C_{11}H_{23}$-melamine + $2C_{11}H_{23}$-melamine	−70082.69

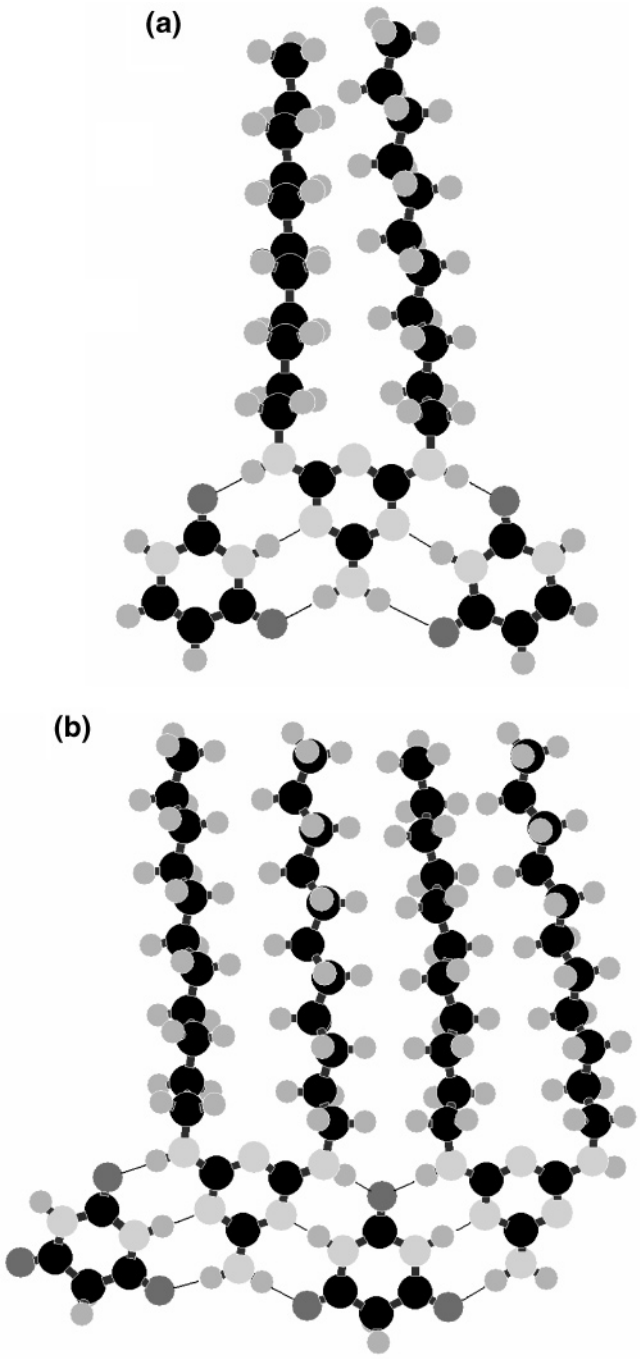

Figure 13. PM3-optimized geometry of the uracil−$2C_{11}H_{23}$-melamine−uracil complex (top) and four molecules of the supramolecular $2C_{11}H_{23}$-melamine−barbituric acid network linearly extended by hydrogen bond interaction (bottom).

between a binding face of $2C_{11}H_{23}$-melamine and uracil or $2C_{11}H_{23}$-melamine and barbituric acid (eqs 1a/1b).

$$E_{H1} = E_{complex1} - E_{uracil} - E_{complex1-uracil} \quad (1a)$$

$$E_{H2} = E_{complex2} - E_{barb} - E_{complex2-barbituric\ acid} \quad (1b)$$

In the case of the $2C_{11}H_{23}$-melamine−barbituric acid entity, the hydrogen bond energy of the doubly bonded barbituric acid was also calculated. The values of energy and length of the hydrogen bonding, which are only slightly dependent on the molecular conformation of the amphiphilic $2C_{11}H_{23}$-melamine, are listed in Table 4. The generally high values of the hydrogen bond energy express the high stability of the supramolecular species. The hydrogen bond energies for the two uracil molecules are not exactly the same (see Table 4) because the conformation of $2C_{11}H_{23}$-melamine is not completely symmetric. It is also seen in Table 4 that the highest values of the hydrogen bond energy were calculated for the two $2C_{11}H_{23}$-melamine molecules bonded with two barbituric acid molecules in alternating sequence (apart from the supramolecular $2C_{11}H_{23}$-melamine−barbituric acid network linearly extended by hydrogen bond interaction). Approximately twice the energy was obtained in the case that the two binding faces of the barbituric acid molecule are complimentarily bound to the two binding faces of $2C_{11}H_{23}$-melamine. The comparatively high hydrogen bond energy obtained for the interfacial $2C_{11}H_{23}$-melamine−barbituric acid assembly is in agreement with its fundamental differences in the morphological and thermodynamic interfacial features in comparison to those of the interfacial $2C_{11}H_{23}$-melamine−thymine/uracil assemblies.

TABLE 4: Energy and Length of Hydrogen Bonds in Supramolecular Species

supramolecular bonding of $2C_{11}H_{23}$-melamine	hydrogen bonds		
	energy [kJ/mol]	length [nm]	
		O···H	H···N
with uracil	−31.85/−32.48	1.86−1.87	1.74
with barbituric acid	−34.428	1.82−1.88	1.74−1.75
with barbituric acid, doubly bonded	−65.758	1.82−1.88	1.74−1.75

Conclusions

Numerous preceding experimental studies of monolayers of versatile chemical structure demonstrated unambiguously that hydrogen-bond-based molecular recognition is highly effective at the air−water interface. However, there has been nearly no information about the effect of the nonsurface-active component dissolved in the aqueous subphase on structure and phase properties of the monolayers of the supramolecular structures formed by complementary hydrogen bonding at the air−water interface.

The present comparison of the main characteristics of Langmuir monolayers of a selected amphiphilic melamine-type molecule 2,4-di(*n*-undecylamino)-6-amino-1,3,5-triazine ($2C_{11}H_{23}$-melamine) with those of the corresponding supramolecular entities by molecular recognition of dissolved nonsurface-active uracil or barbituric acid should be a contribution to fill this gap. The changes in the structural and phase features at the interfacial recognition process can be optimally characterized by the combination of surface pressure studies with Brewster angle microscopy (BAM) imaging and grazing incidence X-ray diffraction (GIXD) measurements.

The molecular recognition of uracil or barbituric acid gives rise to drastic but specific changes in the phase behavior of the $2C_{11}H_{23}$-melamine monolayer and the morphology of the condensed phase domains. Pure $2C_{11}H_{23}$-melamine monolayers show only small compact, but nontextured condensed phase domains, despite the striking two-phase coexistence region of the π−A isotherms in the accessible temperature range. The morphological features of the monolayers of the supramolecular assemblies are highly specific in dependence on, not only the chemical structure of the dissolved pyrimidine derivative, but also a slight modification of the alkyl chain. The condensed phase domains of the $2C_{11}H_{23}$-melamine−uracil assemblies develop pronounced well-shaped circular condensed-phase domains with a striking tendency to two-dimensional Ostwald

ripening. The continuous change in the brightness indicates an inner texture with alkyl chains essentially oriented parallel to the periphery. The morphology of the $2C_{11}H_{23}$-melamine−barbituric acid monolayers is completely different. These assemblies form large homogeneous areas of condensed phase that transfer at smaller areas per molecule to a homogeneous condensed monolayer. BAM imaging of the supramolecular assemblies formed by $((CH_3(CH_2)_{11}O(CH_2)_3)_2$−melamine and uracil or barbituric acid illustrates that a modification of the chemical structure of the alkyl chains affects in a specific way the domain morphology. The characteristics of surface pressure and domain morphology of the interfacial systems can be essentially affected by the kinetics of the recognition process.

The GIXD results reveal that the molecular recognition of pyrimidine derivatives gives rise only to quantitative changes in the two-dimensional lattice structure of the alkyl chains. That means the formation of hydrogen-bond-based superstructures between the polar headgroups of the amphiphilic monolayer and the nonsurface-active species present in the aqueous subphase does not generally change the two-dimensional lattice structure of the alkyl chains.

The striking differences in the main characteristics of the monolayers of the supramolecular structures can be related to their different chemical structures. Complementary hydrogen bonding of two uracil molecules by one $2C_{11}H_{23}$-melamine molecule is concluded from the chemical structure of both components. In the case of barbituric acid, $2C_{11}H_{23}$-melamine can form a linearly extended hydrogen bonding network. Additional information about the nature of the hydrogen-bonding-based supramolecular entities obtained by using quantum chemical PM3 approximation support the results about the specific differences in the monolayer characteristics of the supramolecular structures. Energy and lengths of the hydrogen bonds of the optimized uracil−$2C_{11}H_{23}$-melamine−uracil structure and the linearly extended uracil−barbituric acid network have been calculated.

Acknowledgment. Financial support from the Deutsche Forschungsgemeinschaft (DFG grant VO-710/7-1) is gratefully acknowledged.

References and Notes

(1) Lehn, J.-M. *Angew. Chem., Int. Ed. Engl.* **1990**, *29*, 1304.
(2) Ringsdorf, H.; Schlarb, B.; Venzmer, J. *Angew. Chem., Int. Ed. Engl.* **1989**, *27*, 113.
(3) Boschke, F. L., Ed. Hydrogen bonds. In *Topics in Current Chemistry*; Springer-Verlag: Heidelberg, 1984; Vol. 120.
(4) Alberts, B.; Bray, D.; Lewis, J.; Raff, M.; Roberts, K.; Watson, J. D. *Molecular Biology of the Cell*, 2nd ed.; Garland Publishing: New York, 1989.
(5) Spinke, J.; Liley, M.; Schmitt, F.-J.; Guder, H.-J.; Angermaier, L.; Knoll, W. *J. Chem. Phys.* **1993**, *99*, 7012.
(6) Wenz, G. *Angew. Chem., Int. Ed. Engl.* **1994**, *33*, 803.
(7) Desiraju, G. R. *Angew. Chem., Int. Ed. Engl.* **1995**, *107*, 2541.
(8) Zerkowski, J. A.; MacDonald, J. C.; Seto, C. T.; Wierda, D. A.; Whitesides, G. M. *J. Am. Chem. Soc.* **1994**, *116*, 2382.
(9) Zerkowski, J. A.; Whitesides, G. M. *J. Am. Chem. Soc.* **1994**, *116*, 4298.
(10) Zerkowski, J. A.; Mathias, J. P.; Whitesides, G. M. *J. Am. Chem. Soc.* **1994**, *116*, 4305.
(11) Ikeura, Y.; Kurihara, K.; Kunitake, T. *J. Am. Chem. Soc.* **1991**, *113*, 7342.
(12) Kusmenko, I.; Buller, R.; Bouwman, W. G.; Kjaer, K.; Als-Nielsen, J.; Lahav, M.; Leiserowitz, L. *Science* **1996**, *274*, 2046.
(13) Ariga, K.; Kunitake, T. *Acc. Chem. Res.* **1998**, *31*, 371.
(14) Ebara, Y.; Itakura, K.; Okahata, Y. *Langmuir* **1996**, *12*, 5165.
(15) Matsuura, K.; Ebara, Y.; Okahata, Y. *Langmuir* **1997**, *13*, 814.
(16) Kimizuka, N.; Kawasaki, T.; Kunitake, T. *J. Am. Chem. Soc.* **1993**, *115*, 4387.
(17) Kimizuka, N.; Kawasaki, T.; Kunitake, T. *Chem. Lett.* **1994**, 33.
(18) Shimomura, M.; Nakamura, F.; Ijiro, K.; Taketsuna, H.; Tanaka, M.; Nakamura, H.; Hasebe, K. *J. Am. Chem. Soc.* **1997**, *119*, 2341.
(19) Vollhardt, D.; Liu, F.; Rudert, R.; He, W. *J. Phys. Chem. B* **2005**, *109*, 10849.
(20) Thurston, J. T.; Dudley, J. R.; Kaiser, D. W.; Hechenbleikner, I.; Schaefer, F. C.; Holm-Hanson, D. J. *J. Am. Chem. Soc.* **1951**, *73*, 2981.
(21) Vollhardt, D. *Adv. Colloid Interface Sci.* **1996**, *64*, 143.
(22) Kjaer, K. *Physica B* **1994**, *198*, 100.
(23) Als-Nielsen, J.; Möhwald, H. In *Handbook on Synchrotron Radiation*; Ebashi, S.; Koch, M.; Rubenstein, E., Eds.; Elsevier: Amsterdam, Oxford, New York, Tokyo, 1994; Vol. 4, pp 1−53.
(24) Als-Nielsen, J.; Jacquemain, D.; Kjaer, K.; Lahav, M.; Leiveiller, F.; Leiserwitz, L. *Phys. Rep.* **1994**, *246*, 251.
(25) Als-Nielsen, J.; Kjaer, K. In *Phase Transitions in Soft Condensed Matter*; Riste, T.; Sherrington, D., Eds.; NATO ASI Series B.; Plenum Press: New York, 1989; Vol. 211, p 113.
(26) Weidemann, G.; Vollhardt, D. *Langmuir* **1996**, *12*, 5114.
(27) Vollhardt, D.; Brezesinski, G.; Siegel, S.; Emrich, G. *J. Phys. Chem. B* **2001**, *105*, 12061.
(28) Stewart, J. J. P. *J. Comput. Chem.* **1989**, *10*, 221.